OPEN ACCESS

Original research

Pharmacological activation of STAT1-GSDME pyroptotic circuitry reinforces epigenetic immunotherapy for hepatocellular carcinoma

Yalin Tu,[1] Haoran Wu,[1] Chengpeng Zhong,[1,2] Yan Liu,[1] Zhewen Xiong,[1] Siyun Chen,[1] Jing Wang,[1] Patrick Pak-Chun Wong,[1] Weiqin Yang,[1] Zhixian Liang,[1] Jiahuan Lu,[1] Shufen Chen,[1] Lingyun Zhang,[1] Yu Feng,[1] Willis Wai-Yiu Si-Tou,[1] Baoyi Yin,[1] Yingnan Lin,[1] Jianxin Liang ,[1] Liying Liang,[3] Joaquim S L Vong,[1] Weida Ren,[1] Tsz Tung Kwong,[4] Howard Leung,[5] Ka Fai To,[5] Stephanie Ma ,[6] Man Tong,[1] Hanyong Sun,[2] Qiang Xia,[2] Jingying Zhou ,[1] David Kerr,[7] Nick La Thangue,[8] Joseph J Y Sung ,[9,10] Stephen Lam Chan,[4] Alfred Sze-Lok Cheng [1]

► Additional supplemental material is published online only. To view, please visit the journal online (https://doi.org/10.1136/gutjnl-2024-332281).

For numbered affiliations see end of article.

Correspondence to
Professor Alfred Sze-Lok Cheng; alfredcheng@cuhk.edu.hk and Professor Stephen Lam Chan; chanlam_stephen@cuhk.edu.hk

YT and HW contributed equally.

Received 24 February 2024
Accepted 2 October 2024

To cite: Tu Y, Wu H, Zhong C, *et al*. *Gut* Epub ahead of print: [*please include* Day Month Year]. doi:10.1136/gutjnl-2024-332281

ABSTRACT

Background Genomic screening uncovered interferon-gamma (IFNγ) pathway defects in tumours refractory to immune checkpoint blockade (ICB). However, its non-mutational regulation and reversibility for therapeutic development remain less understood.

Objective We aimed to identify ICB resistance-associated druggable histone deacetylases (HDACs) and develop a readily translatable combination approach for patients with hepatocellular carcinoma (HCC).

Design We correlated the prognostic outcomes of HCC patients from a pembrolizumab trial (NCT03419481) with tumourous cell expressions of all HDAC isoforms by single-cell RNA sequencing. We investigated the therapeutic efficacy and mechanism of action of selective HDAC inhibition in 4 ICB-resistant orthotopic and spontaneous models using immune profiling, single-cell multiomics and chromatin immunoprecipitation-sequencing and verified by genetic modulations and co-culture systems.

Results HCC patients showing higher *HDAC1/2/3* expressions exhibited deficient IFNγ signalling and poorer survival on ICB therapy. Transient treatment of a selective class-I HDAC inhibitor CXD101 resensitised HDAC1/2/3^{high} tumours to ICB therapies, resulting in CD8^{+}T cell-dependent antitumour and memory T cell responses. Mechanistically, CXD101 synergised with ICB to stimulate STAT1-driven antitumour immunity through enhanced chromatin accessibility and H3K27 hyperacetylation of IFNγ-responsive genes. Intratumoural recruitment of IFNγ^{+}GZMB^{+}cytotoxic lymphocytes further promoted cleavage of CXD101-induced Gasdermin E (GSDME) to trigger pyroptosis in a STAT1-dependent manner. Notably, deletion of GSDME mimicked STAT1 knockout in abolishing the antitumour efficacy and survival benefit of CXD101-ICB combination therapy by thwarting both pyroptotic and IFNγ responses.

Conclusion Our immunoepigenetic strategy harnesses IFNγ-mediated network to augment the cancer-immunity cycle, revealing a self-reinforcing STAT1-GSDME pyroptotic circuitry as the mechanistic basis for an ongoing phase-II trial to tackle ICB resistance (NCT05873244).

WHAT IS ALREADY KNOWN ON THIS TOPIC

⇒ Immune checkpoint blockade (ICB)-resistant hepatocellular carcinoma (HCC) has been primarily linked to the immunosuppressive tumour microenvironment (TME) characterised by immune exclusion of cytotoxic lymphocytes.

⇒ The deficiency of IFNγ signalling confers immune evasion by affecting multiple steps of the cancer-immunity cycle, especially the immune effector cell trafficking/infiltration, antigen presentation and tumour cell recognition.

⇒ The output of IFNγ signalling in HCC is lower than in other solid tumours, but genetic mutations in the IFNγ pathway and its downstream effectors are rarely reported in patients with HCC.

⇒ Although the histone deacetylase (HDAC) family represents promising druggable targets to reprogram TME, the lack of in-depth characterisation of epigenomic reprogramming hinders the development of selective HDAC-targeted immunotherapy.

INTRODUCTION

Hepatocellular carcinoma (HCC), currently the third-leading cause of cancer death worldwide, is estimated to directly affect ~1 million people annually by 2025.[1] Although immune checkpoint blockade (ICB) therapies such as antibodies against programmed cell death-1 (PD-1) or its ligand (PD-L1) have revolutionised the treatment paradigm for HCC, the immunosuppressive tumour microenvironment (TME) characterised by immune exclusion of cytotoxic lymphocytes (CTLs) in tumour stroma restricts the clinical benefits of ICB therapies to a minority of HCC patients.[2] The clinical success of atezolizumab (anti-PD-L1) plus bevacizumab (anti-vascular endothelial growth factor A),[3] which has become the new standard of care for HCC,[4]

WHAT THIS STUDY ADD

⇒ HCC patients with *HDAC1/2/3*^{high} tumours exhibited lower levels of IFNγ and T-cell exclusion gene signatures and poorer survival on ICB therapy.

⇒ A selective class-I HDAC inhibitor CXD101 re-sensitised HDAC1/2/3^{high} tumours to ICB by concomitant restoration of multiple rate-limiting steps of the cancer-immunity cycle.

⇒ CXD101 synergised with ICB to stimulate STAT1-driven antitumour immunity through enhanced chromatin accessibility and H3K27 hyperacetylation of IFNγ-responsive genes.

⇒ CXD101-ICB combination therapy-induced tumour cell pyroptosis by cooperative functions of CXD101-induced GSDME expression and IFNγ/STAT1-mediated cleavage by cytotoxic lymphocytes.

HOW THIS STUDY MIGHT AFFECT RESEARCH, PRACTICE OR POLICY

⇒ The successful conversion of the immune-excluded into an inflamed immunotype through epigenetic activation of STAT1-GSDME pyroptotic circuitry provides a mechanistic basis of CXD101 plus anti-PD-1 treatment in patients with ICB-resistant HCC.

⇒ The application of single-cell multiomics analysis in the new phase-II clinical trial (NCT05873244) will advance precision medicine with immuno-epigenetic therapy through identification of predictive biomarkers for responsiveness and durability.

highlights the importance of cotargeting by combination immunotherapy in the context of TME. However, the fact that less than one-third of patients respond remains a major challenge, which demands more effective strategies against the rate-limiting steps of the cancer-immunity cycle for the generation of antitumour immune responses.[5]

Among cancer-intrinsic and cancer-extrinsic mechanisms underlying immunotherapy resistance,[6] the deficiency of interferon-gamma (IFNγ) signalling confers immune evasion by affecting multiple steps of antitumour immunity, especially the immune effector cell trafficking/infiltration, antigen presentation and tumour cell recognition.[7–9] In HCC, the output of IFNγ signalling is lower than in other solid tumours.[10] Importantly, patients with higher baseline IFNγ responsive genes (IRGs) expression have been found to exhibit good response to ICB therapy.[11] Since genetic mutations in the IFNγ pathway and its downstream effectors are rarely reported in patients with HCC, understanding the non-mutational regulation of IFNγ responses may help reinforce the cancer-immunity cycle and augment efficacy of immunotherapy.

Alterations in epigenomic landscapes have now been recognised to drive the development and progression of cancers.[12] Histone deacetylases (HDACs) responsible for histone deacetylation have become important targets for cancer therapeutic development.[13] Several HDAC inhibitors (HDACi) such as vorinostat, panobinostat and romidepsin have been approved by Food and Drug Administration for the treatment of haematological malignancies.[14] However, the non-selective HDACi used in most studies have also shown immunosuppressive side effects in patients.[15] We and others have recently demonstrated the potential of selective HDACi in enhancing ICB efficacy through TME remodelling using preclinical models of solid tumours including HCC.[16–19] Further in-depth characterisation of the cellular and molecular mechanisms by which specific epigenomic reprogramming elicits antitumour immunity is instrumental in rational development and clinical translation of selective HDAC-targeted immunotherapy.

Elucidating the tumour ecosystem at single-cell resolution has markedly improved our understanding of intratumour heterogeneity, cellular and molecular wiring of TME, and therapeutic resistance.[20] Here, we charted the prognostic outcomes of HCC patients in relationship with all the human HDAC isoforms using single-cell RNA sequencing (scRNA-seq) data from an ICB therapy cohort and identified epigenetic drivers associated with ICB resistance. Elucidating the treatment-induced epigenomic remodelling in our preclinical models through single-cell assays for transposase-accessible chromatin-sequencing (scATAC-seq) and chromatin immunoprecipitation-sequencing (ChIP-seq) further revealed the mechanism of action of a selective HDAC inhibitor plus ICB in revitalising IFNγ responses and a highly immunogenic cell death, thus providing a readily translatable strategy to expand the spectrum of patients who can benefit from ICB therapy.

MATERIALS AND METHODS

A detailed description of all methods used in this study can be found in online supplemental information.

RESULTS

Single-cell transcriptomics of HCC patient biopsies identifies *HDAC1/2/3* as predictive markers for poor responders of ICB therapy

To develop a mechanism-based combinatory ICB strategy with selective HDACi, we integrated single-cell analysis of an HCC patient cohort with functional and mechanistic delineation using our established ICB-resistant mouse models and co-culture systems (figure 1A). Based on scRNA-seq of tumour biopsies from our previous phase-II study of pembrolizumab in patients with HBV-related HCC (NCT03419481),[21] we correlated the baseline expression levels of all 18 human HDAC isoforms in tumour cells with the survival outcomes of patients by Cox proportional hazard models with optimal cut-offs (figure 1B). The results showed that patients with higher expression of *HDAC10*, NAD-dependent deacetylase *Sirtuin* (*SIRT*) *1* and *SIRT5* were correlated with better patient survival on anti-PD-1 treatment (figure 1B and online supplemental figure 1), which are consistent with their immunoregulatory roles in cancer.[22–24]

In contrast, higher expression of three class-I HDACs, namely *HDAC1*, *HDAC2* or *HDAC3,* was significantly associated with poorer survival of HCC patients (figure 1B,C). In line with the observed differences in survival outcome, we also noted that *HDAC1/2/3* was highly expressed in the tumour cells of ICB non-responders compared with responders (figure 1D). Notably, we found that *HDAC1/2/3*^{high} tumour cells uniformly exhibited lower levels of IFNγ gene signature (figure 1E). Moreover, Tumour Immune Dysfunction and Exclusion (TIDE) analysis[25] of bulk RNA-seq dataset from The Cancer Genome Atlas (TCGA) also demonstrated highly significant associations of *HDAC1/2/3*^{high} patients with predicted ICB non-responsiveness (figure 1F), further evidenced by the higher TIDE, T cell exclusion and myeloid-derived suppressor cell (MDSC) gene signatures (figure 1G). Overall, these data support the isoform-specific roles of HDAC1/2/3 in antagonising the immune responses of HCC patients to ICB therapy.

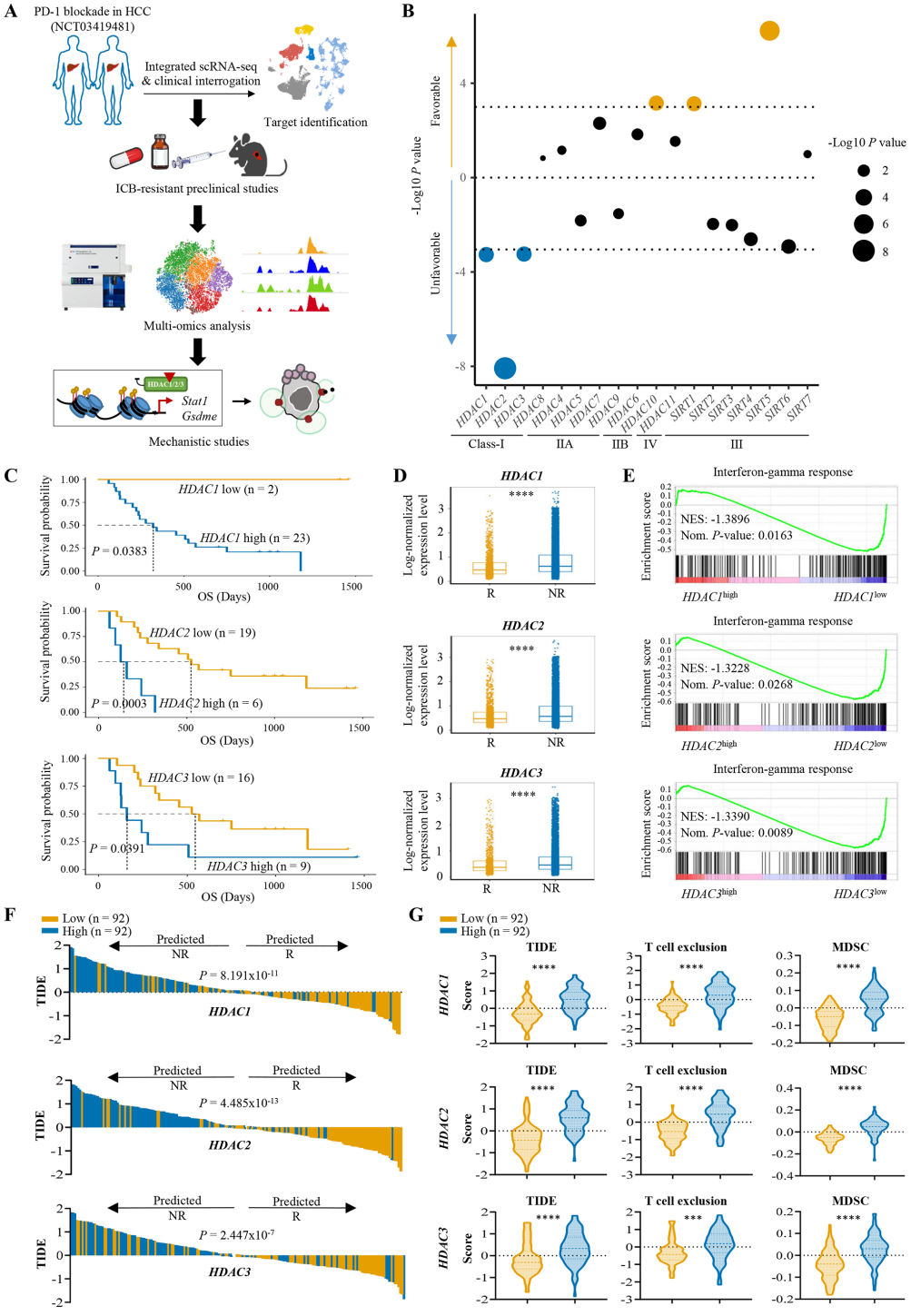

Figure 1 Tumour cell-intrinsic HDACs correlate with ICB therapy efficacy and survival outcome in patients with HCC. (A) Overview of this study. (B) Dot plot depicting the relationship between the baseline expression levels of tumour cell-intrinsic *HDAC* isoforms and the survival outcomes of HCC patients treated with pembrolizumab. Each plot represents a p value obtained from the Kaplan-Meier survival analysis of the patients according to their baseline tumourous cell *HDAC* expression levels. (C) Kaplan-Meier survival analyses of patients with HCC undergone pembrolizumab treatment according to their baseline tumourous cell *HDAC1*, *HDAC2* and *HDAC3* expression levels. (D) Expression levels of *HDAC1*, *HDAC2* and *HDAC3* in tumour cells of the patients according to pembrolizumab treatment outcomes. (E) GSEA of the genes between the *HDAC1/2/3*^{high} and *HDAC1/2/3*^{low} tumour cells. Tumour cells were stratified by top (high) and bottom (low) 25% based on the expression levels of *HDAC1*, *HDAC2* or *HDAC3*. (F, G) TCGA HCC samples with high (n=92) and low (n=92) mRNA levels of *HDAC1*, *HDAC2* or *HDAC3* stratified by top and bottom 25% in 369 patients were selected for subsequent analysis. (F) Prediction of potential clinical ICB response in patients between the *HDAC1/2/3*^{high} and *HDAC1/2/3*^{low} tumour cells using the TIDE signature. R, responders; NR, non-responders. (G) Analysis of TIDE, T cell exclusion and MDSC scores by TIDE algorithm in patients between the *HDAC1/2/3*^{high} and *HDAC1/2/3*^{low} tumour cells. Statistical significance was assessed by two-sided log-rank (Mantel-Cox) test for (B, C), by Wilcoxon rank sum test for (D), by Kolmogorov-Smirnov test for (E), by two-sided χ^2 test for (F) or by unpaired two-tailed Student's t-test for (G). ***p<0.001; ****p<0.0001. HCC, hepatocellular carcinoma; HDAC, histone deacetylase; ICB, immune checkpoint blockade; MDSC, myeloid-derived suppressor cell; NR, non-responders; R, responders; TIDE, Tumour Immune Dysfunction and Exclusion.

A selective class-I HDAC inhibitor resensitises HDAC1/2/3^{high} tumours to ICB by triggering robust antitumour immunity

To recapitulate the insensitivity of ICB in HCC patients, we have established Hepa1-6 and RIL-175 derived anti-PD-L1-resistant (PD-L1R) models by serial orthotopic implantation of HCC cells through anti-PD-L1-treated syngeneic, immunocompetent mice.[21] We also generated RIL-175 derived anti-PD-1-resistant (PD-1R) model using the same in vivo selection approach (online supplemental figure 2A), in which anti-PD-1 treatment no longer exerted a significant effect on the PD-1R tumours (online supplemental figure 2B). Compared with the parental ICB-sensitive HCC cells, the PD-(L)1R-induced TME was composed of fewer CTLs, namely CD4$^+$T, CD8$^+$T, natural killer (NK) and NKT cells with less cytotoxic marker expressions but more MDSCs (online supplemental figure 2C,D).[21] Notably, HDAC1/2/3 was highly expressed in the tumour cells of ICB-resistant mouse models (figure 2A and online supplemental figure 3A,B), which also showed reduced levels of IRG expressions (online supplemental figure 2E) as observed in *HDAC1/2/3*^{high} HCC patients exhibiting poor response to ICB therapy.

Given the pivotal role of IFNγ signalling in cancer immunotherapy,[7–9] we hypothesised that HDAC1/2/3 may confer ICB resistance through dysregulated hepatoma-intrinsic IFNγ signalling. We first investigated the functional effects of a selective HDAC1/2/3 inhibitor, CXD101/zabadinostat,[26 27] in combination with PD-(L)1 blockade in three ICB-resistant orthotopic models (figure 2B). While CXD101 monotherapy showed limited effect, the tumour growth was substantially abrogated when CXD101 treatment was combined with anti-PD-(L)one antibody (figure 2C,D, and online supplemental figure 4), without observable side effect of weight loss or internal organ abnormality (online supplemental figure 5A–G). Moreover, the combination therapy significantly decreased the serum alanine transaminase and aspartate transaminase levels to the extent comparable to that of age-matched normal mice (online supplemental figure 5H). As evidence of CTL-mediated antitumour immunity, coblockade of HDAC1/2/3 and PD-(L)1 significantly increased the intratumoural levels of a key chemokine CXCL10[28] (online supplemental figure 6) and CD45 positive leukocytes (figure 2E, online supplemental figure 7A,8A), mainly composed of CD8$^+$T, CD4$^+$T, NK and NKT cells (figure 2F, online supplemental figure 7A, 8A) which exhibited significantly negative correlations with tumour burden (figure 2G). Of note, the combination of CXD101 and anti-PD-(L)1 also significantly augmented the antitumour functions of CD8$^+$T cells as demonstrated by the increased proportions of IFNγ$^+$ and granzyme B$^+$ (GZMB$^+$) cells (figure 2H and online supplemental figure 7B,8B). Notably, depletion of CD8$^+$T cells, but not NK cells, significantly impeded the combination therapy-induced intratumoural CD45$^+$immune cells infiltration and lytic tumour cell death, leading to abolishment of the therapeutic efficacy (online supplemental figure 9). These findings suggest that the antitumour CD8$^+$T cell functions mediate the combination therapy.

Remarkably, the combination treatment significantly prolonged the mouse survival and resulted in tumour eradication in >50% of mice in the Hepa1-6-PD-L1R model (figure 2I,J). These findings suggest that transient treatment of CXD101 synergises with ICB to induce long-lasting protection that may prevent future recurrence. Indeed, in contrast to the treatment-naïve mice of the same age, all mice cured by prior coblockade survived after a secondary tumour challenge implanted into their livers (figure 2K), which were accompanied by significant increases in effector memory CD8$^+$T cells (CD8$^+$T$_{EM}$) and CD4$^+$T$_{EM}$ cells in the peripheral blood (figure 2L). Overall, these data suggest that HDAC1/2/3 inhibition induces strong antitumour immunity for effective and durable ICB therapies via promoting CTL recruitment, activation and memory formation.

Single-cell multiomics reveals reactivation of IFNγ/STAT1 signalling by CXD101-ICB combination therapy

To decode the molecular and epigenetic reprogramming leading to the therapy-induced antitumour immunity, we performed single-cell multiomics[29] using tumour tissues from the Hepa1-6-PD-L1R model at an earlier treatment time point (day 11) (figure 3A and online supplemental figure 10). We obtained transcriptomic and open chromatin profiles for ~5700–7000 single cells in each of the four control/single/combination treatment groups and identified clusters of tumour cells, lymphocytes, myeloid cells, endothelial cells and fibroblasts based on the canonical markers (figure 3B–D and online supplemental figure 11A,B). While the immune cell proportions were markedly increased by the combination treatment, the tumour cell proportion was greatly reduced (figure 3E). However, reclustering of the tumour cells based on RNA expression (figure 3F and online supplemental figure 12A) and chromatin accessibility profiles (figure 3G and online supplemental figure 12B) revealed distinctive increases in the C6-RNA and C6-ATAC subclusters, respectively (figure 3H–K), which were enriched in interferon-related immue effector functions (figure 3L,M). Moreover, >70% (433) of genes associated with the C6-ATAC subcluster overlapped with the C6-RNA genes (figure 3N) and similarly enriched in response to type II interferon and MHC class-I peptide loading complex (figure 3O). Transcriptional Regulatory Relationships Unravelled by Sentence-based Text mining[30] further predicted that the overlapping genes were predominantly regulated by transcription factors crucial for IFNγ-dependent immunity (figure 3P), namely signal transducer and activator of transcription 1 (STAT1) and interferon regulatory factor 1 (IRF1) that were concomitantly upregulated in the C6-RNA subcluster (figure 3Q).

Gene set enrichment analysis (GSEA) confirmed the significant enrichment of IFNγ response as the top pathway induced by the CXD101-ICB combination therapy when compared with the control group (figure 3R). In concord, the expressions of IRGs related to antigen processing and presentation (*B2m*, *Cd74*, *Tap1* and *Tapbp*), lymphocyte recruitment (*Cxcl9* and *Cxcl10*) and signalling transduction (*Stat1* and *Irf1*) were synergistically upregulated (figure 3S and online supplemental figure 13A–C) and accompanied by increased chromatin accessibilities (figure 3T). ATAC-based motif analysis further highlighted remarkable enrichments of the STAT/IRF families, which were not observed in the comparisons with single treatment by CXD101 or anti-PD-L1 (figure 3U and online supplemental figure 14). Collectively, these data demonstrate that CXD101 synergises with ICB to reactivate IFNγ/STAT1 signalling to induce IRG expressions in a subset of tumour cells, which may contribute to the antitumour responses.

H3K27 hyperacetylation by CXD101 primes IRG activation in response to ICB-induced IFNγ

IFNγ augments the transcriptional activation of IRGs by opening and priming chromatin with positive histone marks at the gene regulatory elements.[8] Surprisingly, the intratumoural IFNγ levels induced by anti-PD-(L)1 were not significantly different from anti-PD-(L)1 plus CXD101 in ICB-resistant models (online supplemental figure 15A,B), indicating that IFNγ immune

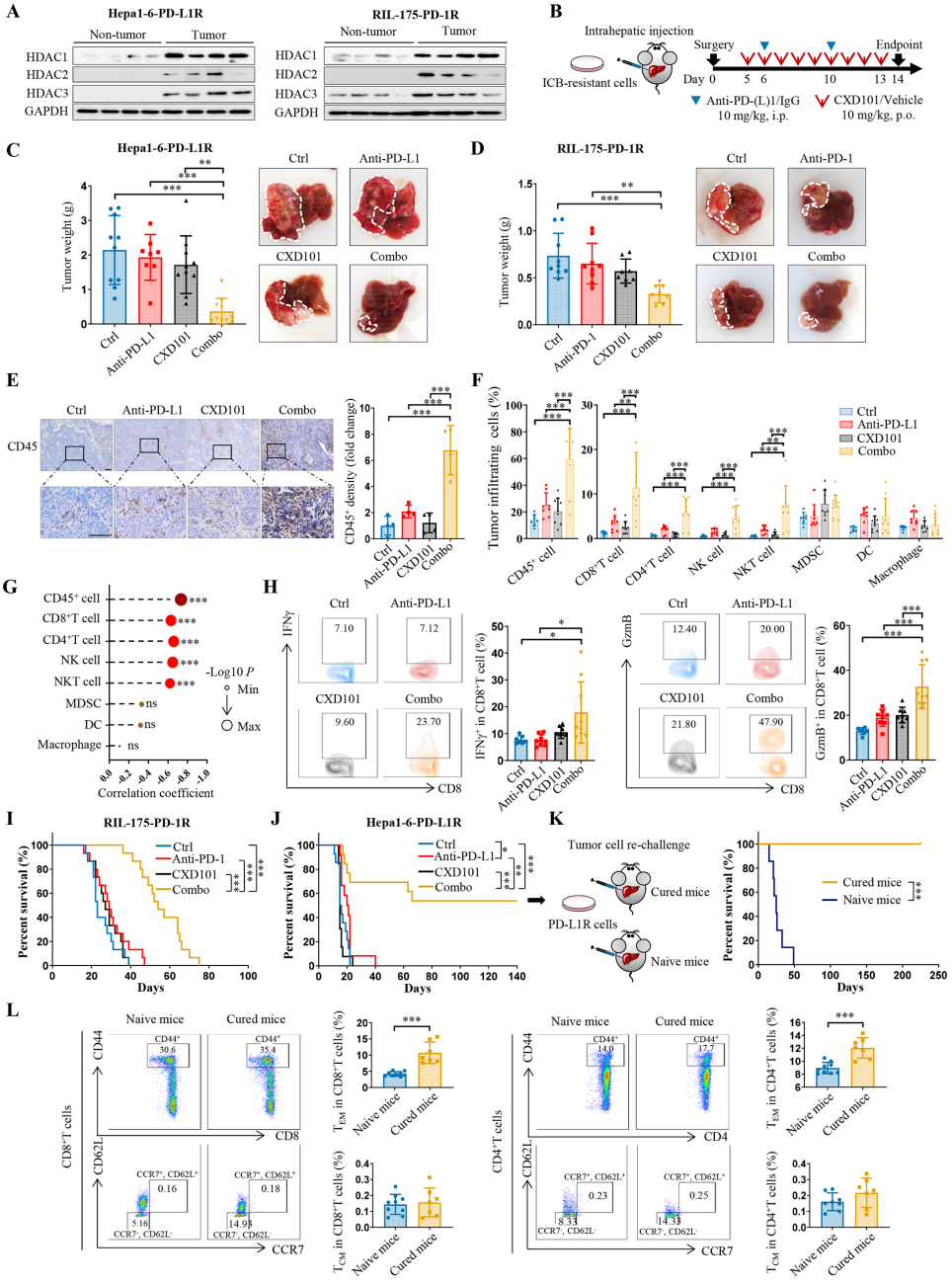

Figure 2 A selective class-I HDAC inhibitor overcomes ICB resistance in HCC models. (A) Western blot analysis of HDAC1, HDAC2 and HDAC3 levels in orthotopic Hepa1-6-PD-L1R (left) and RIL-175-PD-1R (right) tumour and non-tumour liver tissues isolated from mice. GAPDH was used as loading control. (B) Treatment schedule of CXD101 and anti-PD-(L)1 antibody in C57BL/6 mice bearing PD-(L)1R tumours. (C, D) Tumour weights and representative images of livers and tumours from indicated groups in Hepa1-6-PD-L1R (C) and RIL-175-PD-1R (D) models (n=8–10). (E) Representative CD45 immunohistochemistry images and statistical analysis of positively stained cells in Hepa1-6-PD-L1R tumours from indicated groups (n=4). Scale bars, 100 µm. Black boxes indicate regions shown in enlarged inset. (F) Proportions (%) of tumour infiltrating $CD45^+$cells, $CD45^+CD3^+CD8^+$T cells, $CD45^+CD3^+CD4^+$T cells, $CD45^+NK1.1^+$NK cells, $CD45^+CD3^+NK1.1^+$NKT cells, $CD45^+CD11b^+Gr1^+$MDSCs, $CD45^+CD11b^+Gr1^-CD11c^+$dendritic cells, $CD45^+CD11b^+Gr1^-F4/80^+Ly6C^-$ macrophages of total cells in Hepa1-6-PD-L1R tumours from indicated groups were determined by flow cytometry (n=7–9). (G) Correlation analysis between tumour weights and the proportions of indicated cells in Hepa1-6-PD-L1R tumours. (H) Representative flow cytometry dot plots and proportions of $IFN\gamma^+$ or $GZMB^+$ cells in tumour infiltrating $CD8^+$T cells from indicated groups in Hepa1-6-PD-L1R model (n=7–9). (I, J) Kaplan-Meier survival analysis of mice from indicated groups in RIL-175-PD-1R (I) and Hepa1-6-PD-L1R (J) ICB-resistant models (n=12–15). (K) Combination therapy cured mice (from J) and naïve mice with same age were challenged with Hepa1-6-PD-L1R cells at 140 days after initial tumour cell inoculation (n=7). Kaplan-Meier survival analysis of mice from indicated groups are shown. (L) Representative flow cytometry dot plots and proportions of $CD8^+CD44^+CCR7^+CD62L^+$central memory $CD8^+$T cells ($CD8^+T_{CM}$) and $CD8^+CD44^+CCR7^-CD62L^-$effector memory $CD8^+$T cells ($CD8^+T_{EM}$) in circulating $CD8^+$T cells, and the corresponding $CD4^+T_{CM}$ and $CD4^+T_{EM}$ in circulating $CD4^+$T cells from combination therapy cured mice and naive mice (n=7). Data are represented as mean±SD. Statistical significance was assessed by one-way ANOVA with Tukey's multiple comparisons correction for (C–F, H), by single-tailed Pearson's correlation for (G), by two-sided log-rank (Mantel-Cox) test for (I–K) or by unpaired two-tailed Student's t-test for (L). ns, no significance; *p<0.05; **p<0.01; ***p<0.001. ANOVA, analysis of variance; HCC, hepatocellular carcinoma; HDAC, histone deacetylase; ICB, immune checkpoint blockade.

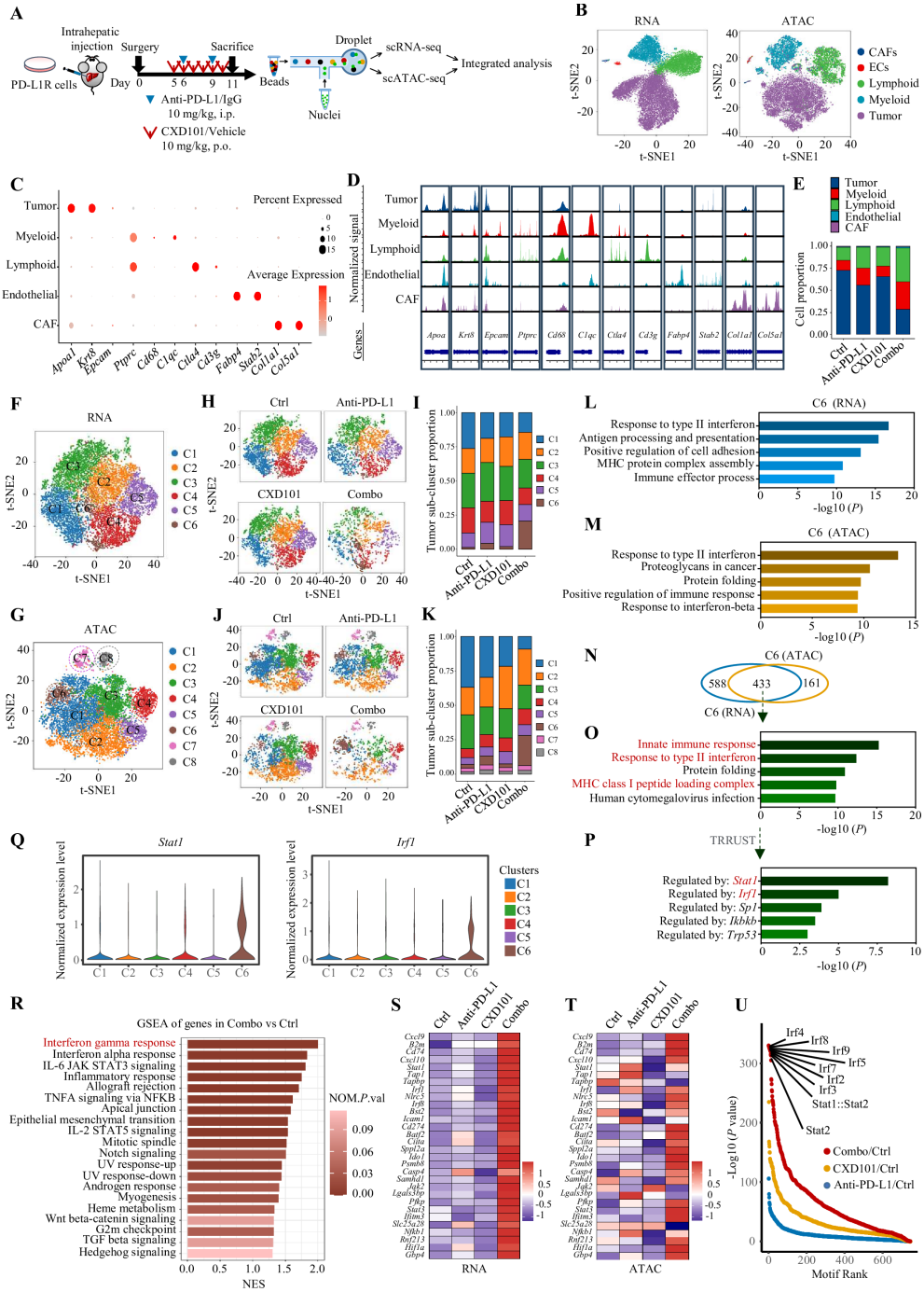

Figure 3 Single-cell multiomics reveals reactivation of IFNγ/STAT1 signalling by CXD101-ICB combination therapy. (A) Treatment schedule of CXD101 and anti-PD-L1 antibody in mice bearing Hepa1-6-PD-L1R tumours for single-cell multiomics analysis. Fresh tumour tissues from three representative mice per group were employed to avoid the interindividual variability. (B) t-SNE plot showing identified cell clusters within tumour from all merged groups. Cell annotations were derived from RNA analysis according to representative lineage markers. (C) Dot plot showing the RNA expression levels of representative marker genes in annotated cell clusters. (D) Visualisation of the pseudo bulk chromatin accessibility tracks of representative marker gene loci in annotated cell clusters. (E) Distribution fraction of distinct cells in the indicated groups. (F, G) t-SNE plot showing the identified subclusters of tumour cells from RNA (F) and ATAC (G). (H, I) t-SNE plots (H) and proportions (I) of the identified tumour sub-clusters in indicated groups from RNA analysis. (J, K) t-SNE plots (J) and proportions (K) of identified tumour subclusters in indicated groups from ATAC analysis. (L, M) Pathway enrichment of differentially expressed genes for RNA-based cluster 6 (C6 (RNA)) (L) and ATAC-based cluster 6 (C6 (ATAC)) (M), respectively. (N) Overlapping genes between C6 (RNA) and C6 (ATAC). (O) Pathway enrichment of overlapping genes in (N). (P) TRRUST analysis showing the key transcription factors for regulating the overlapping genes. (Q) Violin plots showing the RNA expression levels of *Stat1* and *Irf1* across the six tumour cell subclusters based on scRNA-seq analysis. (R) GSEA of the genes in combination group versus control group. (S, T) Heatmap for the RNA expression (S) and chromatin accessibility (T) levels of the top 30 IRGs (upregulated in combination therapy-treated group) in tumour cells from indicated groups. (U) Transcription factor-binding motif enrichment analysis showing the key transcription factors in tumour cells of the indicated groups versus control group. ICB, immune checkpoint blockade; TRRUST, Transcriptional Regulatory Relationships Unravelled by Sentence-based Text mining.

stimulus alone is not sufficient to elicit full antitumour responses, which may be due to alterations of the epigenomic landscape in the ICB-resistant tumour cells. To understand how CXD101 resensitises tumourous responsiveness to ICB-induced IFNγ stimulation, we investigated the chromatin remodelling of tumour tissues from the Hepa1-6-PD-L1R model by ChIP-seq of histone H3 lysine 27 acetylation (H3K27ac), H3K4 monomethylation (H3K4me1) and H3K4me3 that distinguish active from inactive/poised enhancer and promoter elements.[31] Intriguingly, treatment with CXD101 alone or in combination with anti-PD-L1 did not obviously alter the genomic distribution of H3K27ac abundance (figure 4A), but substantially increased the H3K27ac levels around the transcription start site of the IRGs (figure 4B) whose chromatin was highly accessible after the combination therapy (figure 3T). For example, CXD101 elevated the H3K27ac level of the H3K4me3-marked promoter of *Cd74*, a crucial effector for antigen presentation,[32] and its H3K27ac level and accessibility were further increased by combination therapy (figure 4C). These results suggest that CXD101-induced H3K27 hyperacetylation primes IRGs for increased chromatin accessibility and robust transcription in response to ICB-induced IFNγ.

The expression, phosphorylation and the subsequent autoregulation of the primary IFNγ signalling mediator STAT1 play a critical role in IRG expressions.[33] As ChIP-seq revealed a CXD101-induced H3K27 hyperacetylation pattern in the open chromatin of the *Stat1* promoter and enhancer (figure 4D), we further investigated the regulatory effect of CXD101 on STAT1 in PD-(L)1 R cells with or without IFNγ stimulation that modelled ICB in vivo. We found that CXD101 dose-dependently amplified STAT1 expression and phosphorylation in the presence of IFNγ (figure 4E, online supplemental figure 16A,B), leading to synergistic upregulation of IRGs (figure 4F, online supplemental figure 6C,D) that mimicked the combination therapy in vivo (online supplemental figure 13A–C). However, CXD101 treatment alone could not activate STAT1 signalling and IRG transcription to the same extent (figure 4E,F and online supplemental figure 16), suggesting that chromatin priming by CXD101 is necessary but not sufficient for full IRG activation in PD-(L)1 R cells. Notably, CRISPR-mediated knockout (KO) of STAT1 (figure 4G) abrogated H3K27ac induction by IFNγ and diminished H3K27ac hyperacetylation in the combined treatment with CXD101 in the *Stat1* promoter and enhancer (figure 4H), leading to the abolishment of synergistic activation of *Stat1* and the other IRG expressions (figure 4I). Altogether, these results provide a synergy mechanism whereby CXD101 cooperatively creates a primed chromatin environment with IFNγ/STAT1 signalling to augment IRG transcription.

CXD101 and IFNγ/STAT1 signalling coordinate CD8$^+$T cell-induced pyroptosis

Given the synergistic activation of IRGs, we next determined whether and how CXD101 and IFNγ/STAT1 signalling coordinate tumour cell killing by CTLs. We briefly cultured the pretreated Hepa1-6-PD-L1R tumour cells with activated CD8$^+$T cells (6 hours) isolated from mice bearing the same parental tumour (figure 5A). We noted that single or combined CXD101 and IFNγ treatment per se did not affect tumour cell viability, whereas concomitant treatment with the CD8$^+$T cells significantly induced tumour cell killing (figure 5B). Notably, the dying tumour cells exhibited swelling and membrane blebbing resembling pyroptotic cell death[34] (figure 5C). Indeed, CXD101 and IFNγ synergistically increased the extracellular level of lactate dehydrogenase (LDH), an enzyme released through membrane permeabilisation by dead or dying cells during pyroptosis, in the presence of CD8$^+$T cells (figure 5D). Moreover, the tumour cell viability was restored in STAT1-KO cells (figure 5E), while the membrane blebbing (figure 5F) and LDH release were also abolished (figure 5G), illustrating that IFNγ/STAT1 signalling is instrumental in CD8$^+$T cell-induced pyroptosis.

Tumour cell recognition by CD8$^+$T cells mediated through IFNγ/STAT1 signalling is fundamental to successful ICB therapy.[7–9] Given the synergistic upregulation of IRGs crucial for MHC class-I complex and antigen presentation (figure 3S and online supplemental figure 13), we next determined the functional effects of CXD101 and IFNγ treatment on tumour cell recognition using an ovalbumin (OVA)-specific, CD8$^+$T (OT-I) cell model (online supplemental figure 17A,B). We found that single or combined CXD101 and IFNγ treatment per se did not affect tumour cell viability, whereas concomitant treatment with the OT-I cells significantly induced OVA-specific tumour cell killing (online supplemental figure 17C). Moreover, the tumour cell viability was restored in STAT1-KO cells (online supplemental figure 17D), illustrating that IFNγ/STAT1 signalling is instrumental in tumour cell recognition by CD8$^+$T cells for effective combination treatment.

As a lytic proinflammatory type of cell death, pyroptosis is induced by the activation and cleavage of pore-forming effector proteins called gasdermins (GSDMs).[35] The family comprises *GSDMA*, *GSDMB*, *GSDMC*, *GSDMD* and *GSDME* in humans, while mice lack *Gsdmb*.[35] Integrated omics analysis of the PD-L1R model revealed chromatin accessibility and H3K27ac occupancy in the regulatory elements of *Gsdmd* and *Gsdme* (online supplemental figure 18). While GSDMD was constitutively expressed in PD-L1R tumour cells in vitro (figure 5H), GSDME was inducible by CXD101 (figure 5I and online supplemental figure 19) with elevated H3K27ac levels at its promoter and enhancer (figure 5J). Intriguingly, GSDME was further cleaved to form its cytotoxic N-terminal domain when the CXD101 and IFNγ-pretreated cells were exposed to CD8$^+$T cells (figure 5H). Moreover, deletion of STAT1 abrogated GSDME cleavage without influencing its induction (figure 5K). Collectively, these results suggest that tumour cell pyroptosis occurs by cooperative functions of CXD101-induced GSDME expression and IFNγ/STAT1-mediated cleavage by CD8$^+$T cells on tumour cell recognition.

GSDME upregulation by CXD101 renders CTL-induced pyroptosis

We further investigated the role of CXD101-induced GSDME expression on CTL-mediated tumour cell pyroptosis using the NK92 cell model,[36] which acquires the capability to recognise and kill mouse tumour cells[37]. We found that pretreatment of Hepa1-6-PD-L1R cells with CXD101 markedly enhanced NK92 cell-induced morphological changes (figure 6A) and LDH release (figure 6B), which phenocopied the pyroptotic effects of GSDME overexpression (figure 6C–E). Consistent with the CD8$^+$T cell model, CXD101 induced cleavage of GSDME, but not GSDMD, and release of a pyroptosis marker high mobility group box 1 (HMGB1)[38] in the medium when the pretreated Hepa1-6-PD-L1R cells were co-cultured with NK92 cells (figure 6F). Notably, CRISPR-mediated KO of GSDME abolished CXD101-induced release of HMGB1 (figure 6G) and LDH (figure 6H) as well as pyroptotic morphological changes even in the presence of NK92 cells (figure 6I). These data suggest that GSDME upregulation by CXD101 renders CTL-induced pyroptosis.

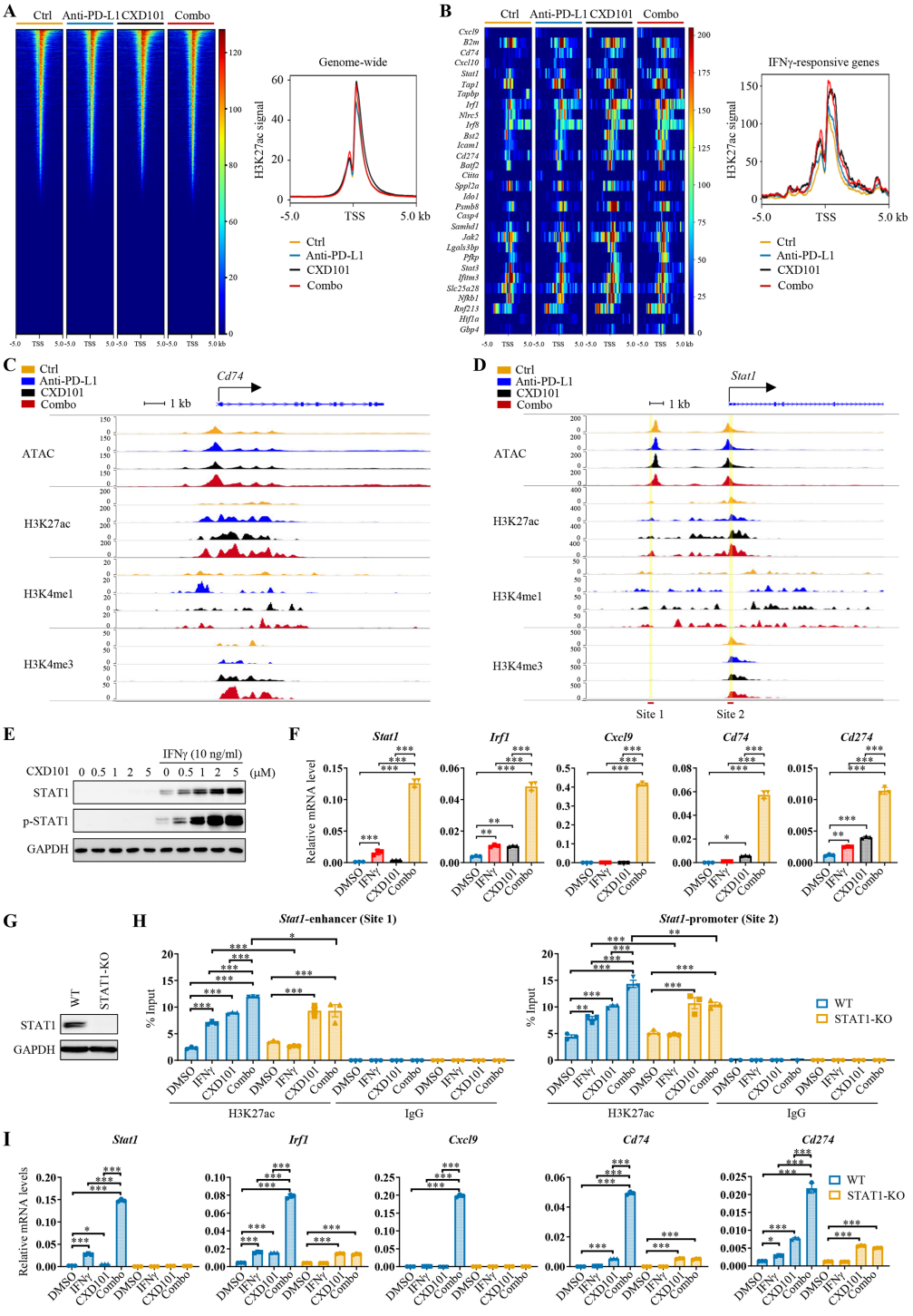

Figure 4 CXD101-induced histone hyperacetylation primes IRG activation in response to IFNγ. (A, B) Heatmaps depicting the H3K27ac intensity in genome-wide scale (A) and in IRGs (B) in tumour tissues from the indicated groups as shown in figure 3A. (C, D) Overlapping tracks of ATAC-seq and nanoscale ChIP-seq (H3K27ac, H3K4me1 and H3K4me3) at the *Cd74* (C) and *Stat1* (D) loci. ATAC-seq data were extracted from the in vivo scATAC-seq of tumour cells. (E) Western blot analysis of STAT1 and p-STAT1 levels in Hepa1-6-PD-L1R cells treated with the indicated concentrations of CXD101 or vehicle control in the presence or absence of IFNγ (10 ng/mL) for 48 hours. GAPDH was used as loading control. (F) RT-qPCR analyses of mRNA levels of the indicated genes in Hepa1-6-PD-L1R cells treated with CXD101 (2 μM) or vehicle control in the presence or absence of IFNγ (10 ng/mL) for 48 hours. *Gapdh* was used as normalisation control. (G) Western blot analysis of STAT1 levels in Hepa1-6 derived PD-L1R-WT and STAT1-KO cells treated with IFNγ (10 ng/mL) for 48 hours. GAPDH was used as loading control. (H) ChIP-qPCR analyses of H3K27ac occupancy in the enhancer and promoter regions of *Stat1* in Hepa1-6 derived PD-L1R-WT or STAT1-KO cells treated with CXD101 (2 μM) or vehicle control in the presence or absence of IFNγ (10 ng/mL) for 48 hours. *Stat1* enhancer (site 1) and promoter (site 2) loci for ChIP-qPCR analysis as shown in figure 4D. (I) RT-qPCR analyses of mRNA levels of the indicated genes in Hepa1-6 derived PD-L1R-WT or STAT1-KO cells treated with CXD101 (2 μM) or vehicle control in the presence or absence of IFNγ (10 ng/mL) for 48 hours. *Gapdh* was used as normalisation control. Data are represented as mean±SEM. Statistical significance was assessed by one-way ANOVA with Tukey's multiple comparisons correction. *p<0.05; **p<0.01; ***p<0.001. ANOVA, analysis of variance; ChIP, chromatin immunoprecipitation.

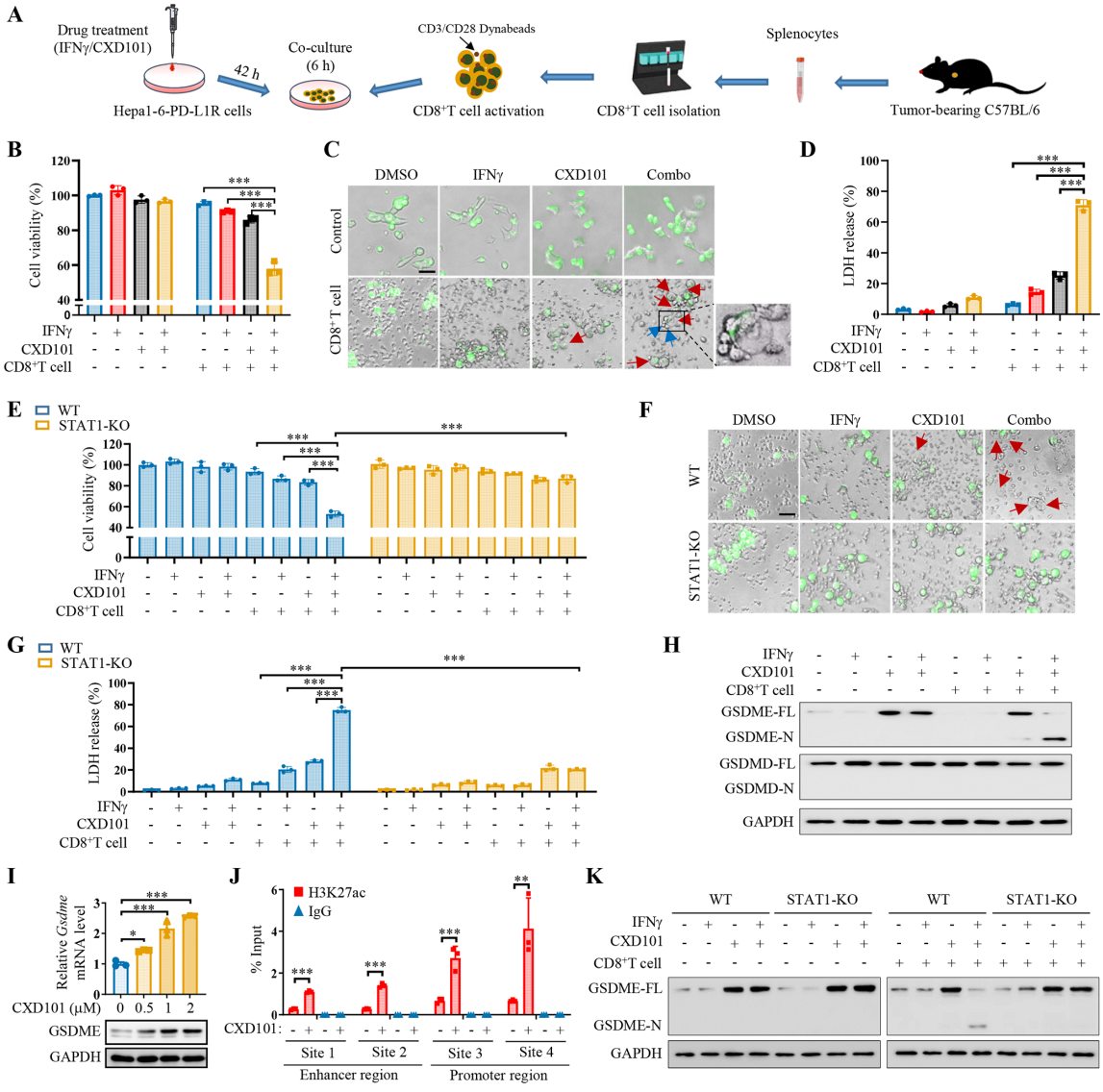

Figure 5 CXD101 and IFNγ/STAT1 signalling coordinate CD8$^+$T cell-induced pyroptosis. (A) Schematic illustration of CD8$^+$T cell/tumour cell co-culture cytotoxicity system. (B–D) Hepa1-6-PD-L1R cells were pretreated with CXD101 (2 μM) or vehicle control in the presence or absence of IFNγ (10 ng/mL) for 42 hours. CD8$^+$T cells at an effector/target ratio (E/T) of 10:1 were co-cultured with drug washed out cells for 6 hours. Cell viabilities (B) morphological changes (C) and LDH release (D) of tumour cells were measured by the corresponding assays. (C) Red arrowheads indicate pyroptotic cells, while blue arrowheads indicate representative CD8$^+$T cells binding on pyroptotic tumour cells. Scale bar=20 μm. (E–G) Hepa1-6 derived PD-L1R-WT or STAT1-KO cells were pretreated with CXD101 (2 μM) or vehicle control in the presence or absence of IFNγ (10 ng/mL) for 42 hours, CD8$^+$T cells at an E/T of 10:1 were co-cultured with drug washed out cells for 6 hours. Cell viabilities (E) morphological changes (F) and LDH release (G) of tumour cells were measured by the corresponding assays. (F) Red arrowheads indicate pyroptotic cells, scale bar=20 μm. (H) Hepa1-6-PD-L1R cells were pre-treated with CXD101 (2 μM) or vehicle control in the presence or absence of IFNγ (10 ng/mL) for 42 hours. CD8$^+$T cells at an E/T of 10:1 were co-cultured with drug washed out cells for 6 hours, followed by Western blot analysis of the indicated proteins. (I) Hepa1-6-PD-L1R cells were treated with DMSO or CXD101 at the indicated concentrations for 48 hours, the *Gsdme* mRNA and GSDME protein levels were measured by RT-qPCR and Western blot assays, respectively. (J) ChIP-qPCR analysis of H3K27ac occupancy in the enhancer and promoter regions of *Gsdme* in Hepa1-6-PD-L1R cells treated with CXD101 (2 μM) or vehicle control for 48 hours. *Gsdme* enhancer and promoter loci for ChIP-qPCR analysis are shown in online supplemental figure 18. (K) Hepa1-6 derived PD-L1R-WT or STAT1-KO cells were pretreated with CXD101 (2 μM) or vehicle control in the presence or absence of IFNγ (10 ng/mL) for 42 hours. CD8$^+$T cells at an E/T of 10:1 were co-cultured with drug washed out cells for 6 hours, followed by Western blot analysis of the indicated proteins. Data are represented as mean±SEM. Statistical significance was assessed by one-way ANOVA with Tukey's multiple comparisons correction. *p<0.05; **p<0.01; ***p<0.001. ANOVA, analysis of variance; ChIP, chromatin immunoprecipitation; LDH, lactate dehydrogenase.

We next examined whether tumour cell pyroptosis occurred on CXD101 and ICB treatment in vivo, by which tumour regression was accompanied by significant recruitment of CTLs (figure 2H). In PD-(L)1R models, we found that the combination treatment induced upregulation and cleavage of GSDME (figure 6J,Kand online supplemental figure 20) and increased proportions of 7-aminoactinomycin (7-AAD)$^+$Annexin V$^+$CD45$^-$cells (figure 6L,M) representing pyroptotic tumour cells,[39] which were accompanied with elevated HMGB1 levels in the TME (figure 6N,O). Taken together with the in vitro data,

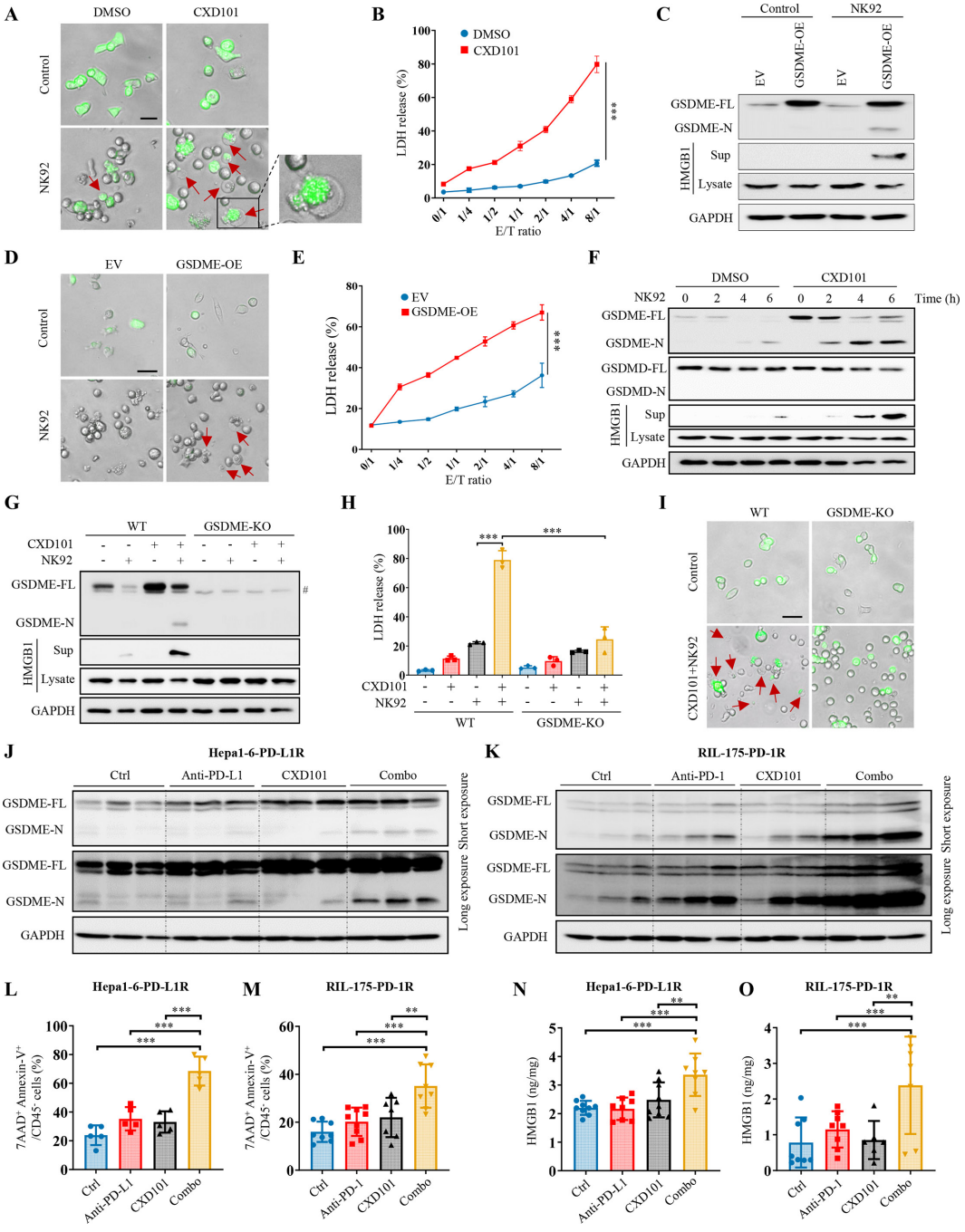

Figure 6 Epigenetic upregulation of GSDME renders CTL-induced tumour cell pyroptosis. (A) Hepa1-6-PD-L1R cells were pretreated with DMSO or CXD101 at 2 µM for 42 hours. NK92 cells at an E/T of 2:1 were co-cultured with drug washed out cells for 5 hours. The representative images are shown. Red arrowheads indicate pyroptotic cells. Scale bar=20 µm. (B) Hepa1-6-PD-L1R cells were pretreated with DMSO or CXD101 at 2 µM for 42 hours. NK92 cells at indicated E/T were co-cultured with drug washed out cells for 5 hours. The LDH release levels of tumour cells are shown. (C–E) Hepa1-6 derived PD-L1R-empty vector (EV) and GSDME-overexpressed (OE) cells were co-cultured with NK92 cells at an E/T of 2:1 for 5 hours. The indicated protein levels (C) morphological changes (D) and LDH release (E) of tumour cells were measured by the corresponding assays. (D) Red arrowheads indicate pyroptotic cells. Scale bar=20 µm. (F) Hepa1-6-PD-L1R cells were pretreated with DMSO or CXD101 at 2 µM for 42 hours. NK92 cells at an E/T of 2:1 were co-cultured with drug washed out cells for the indicated times, followed by Western blot analysis of the indicated proteins. (G) Hepa1-6 derived PD-L1R-WT or GSDME-KO cells were pretreated with DMSO or CXD101 at 2 µM for 42 hours. NK92 cells at an E/T of 2:1 were co-cultured with drug washed out cells for 5 hours. The indicated protein levels (G) LDH release (H) and morphological changes (I) of tumour cells were measured by the corresponding assays. #, non-specific bands. (I) Red arrowheads indicate pyroptotic cells. Scale bar=20 µm. (J, K) The total and cleaved GSDME levels in Hepa1-6-PD-L1R (J) and RIL-175-PD-1R (K) tumours from indicated groups were measured by Western blot assays. GAPDH was used as loading control. (L, M) The proportions of $CD45^-7AAD^+Annexin\text{-}V^+$cells in Hepa1-6-PD-L1R (L) and RIL-175-PD-1R (M) tumours from the indicated groups were detected by flow cytometry assay (n=5–8). (N, O) HMGB1 levels in Hepa1-6-PD-L1R (N) and RIL-175-PD-1R (O) tumours from the indicated groups are shown (n=6–9). Data are represented as mean±SEM (B, E, H) or SD (L–O). Statistical significance was assessed by one-way ANOVA with Tukey's multiple comparisons correction. **p<0.01; ***p<0.001. 7-AAD, 7-aminoactinomycin; ANOVA, analysis of variance; LDH, lactate dehydrogenase.

these findings suggest that intratumoural recruitment and activation of CTLs promote cleavage of CXD101-induced GSDME to trigger pyroptosis in the ICB combination therapy.

Deletion of GSDME abolishes CXD101-ICB combination therapeutic effects by thwarting pyroptotic and IFNγ responses

To investigate the significance of GSDME-triggered pyroptosis and STAT1-mediated IFNγresponses on the combination therapy, we determined the therapeutic efficacy in the Hepa1-6-PD-L1R model derived from wild-type (WT), GSDME-KO and STAT1-KO tumour cells (figure 7A). Notably, deletion of GSDME abolished the antitumour effect of CXD101 and anti-PD-L1 combination treatment to the same extent as the STAT1 KO (figure 7B). Intriguingly, GSDME KO not only abrogated tumour cell pyroptosis as reflected by 7-AAD$^+$Annexin V$^+$CD45$^-$cell proportions (figure 7C,D), but also attenuated the intratumoural IFNγ induction (figure 7E) and IRG upregulations for antigen processing and presentation (*Cd74*, *H2-k1*, *Tap2* and *Tapbp*) by the combination therapy (figure 7F). In addition, the intratumoural recruitment and activation of CTLs were dramatically reduced (figure 7G,H) that ultimately culminated in worsened survival of mice (figure 7I). These findings emphasise the crucial role of GSDME-triggered pyroptosis in tumour cell killing and IFNγ responses for the therapeutic benefits of CXD101 plus anti-PD-L1 treatment.

On the other hand, although deletion of STAT1 did not significantly affect *Gsdme* induction by the combination treatment (figure 7C), the tumour cell pyroptosis was still abolished (figure 7D) which may be attributable to the effect on IFNγ/STAT1-mediated cleavage of GSDME by CD8$^+$T cells as observed in vitro (figure 5). In concord, STAT1 KO dampened the IFNγ induction in TME and IRG upregulations for antitumour immunity (figure 7E–H), leading to a significant reduction in survival benefit of the combination therapy (figure 7I). Taken together, our findings uncover a reciprocal regulation between GSDME-triggered pyroptosis and STAT1-mediated IFNγ responses that plays a pivotal function in the TME remodelling for the effectiveness of the CXD101-ICB combination therapy.

CXD101 averts ICB resistance in spontaneous HDAC1/2/3^{high} HCC model

Given the importance of tumour heterogeneity for resistance to cancer therapies,[40] finally, we tested the efficacy of the combination immunotherapy in a spontaneous HCC model induced by hydrodynamic tail-vein injection (HDTVi) of MYC and CTNNB1 encoding plasmids together with a sleeping beauty transposase construct.[41] We employed this model because it recapitulates the high-frequency mutation and activation of β-catenin pathway observed in human HCCs which are characterised by T cell exclusion and immunotherapy resistance.[42 43] Importantly, data from transcriptomic analysis of 9 HDTVi models[41] showed that the MYC/CTNNB1 tumour model highly expressed *Hdac1/2/3* (figure 8A), which could be validated by Western blot analysis (figure 8B).

Consistent with the previous findings, we first confirmed that the HDAC1/2/3^{high} HCC tumours of the MYC/CTNNB1 model were resistant to anti-PD-L1 therapy (figure 8C,D). Moreover, single CXD101 treatment also did not influence the tumour burden of this aggressive model, which was indicated by the liver weight, liver/body weight ratio and tumour area assessed by H&E staining (figure 8D,E). Remarkably, concurrent CXD101 treatment could re-sensitise HDAC1/2/3^{high} HCC tumours to PD-L1 blockade, resulting in significant reduction in tumour burden (figure 8D,E) and prolongation of mouse survival when compared with the untreated and single treatment groups (figure 8F) without signs of toxicity (online supplemental figure 21). These findings demonstrate that selective class-I HDAC inhibition can overcome ICB resistance in a preclinical model representing the highly prevalent MYC^{high} and CTNNB1^{mut} human HCCs.

DISCUSSION

Recent progress from therapeutic checkpoint inhibition in the clinic has provided new insights into the rate limiting steps of the cancer-immunity cycle.[44] One of the key mechanisms that render the immune system unable to control tumour growth is the deficiency in IFNγ signalling. Despite intensive research on the perturbations of this pathway in cancer patients unresponsive to ICB,[11 45 46] its non-mutational regulation and potential reversibility for therapeutic development remain less understood. Here, our integrated scRNA-seq and clinical interrogation of a PD-1 blockade cohort reveals that HCC patients with *HDAC1/2/3*^{high} tumours exhibited deficient IFNγ signalling and poor survival on ICB therapy. Using our anti-PD-(L)1-resistant orthotopic HCC models and multiomics analysis, we demonstrate the rationality, effectiveness and mechanism of action of selective HDAC1/2/3 inhibition by CXD101, which epigenetically overcomes ICB resistance by activating a self-reinforcing circuitry of IFNγ/STAT1 signalling and GSDME-mediated pyroptosis (figure 8G). More importantly, the CXD101-ICB combination therapy elicited strong antitumour efficacy and survival benefit in a preclinical model of the highly prevalent MYC^{high} and CTNNB1^{mut} human HCCs, thus providing a proof of concept for our ongoing phase-II trial to tackle resistance to ICB treatment in HCC (NCT05873244).

The iterative nature of the antitumour immune responses where the recognition and killing of tumour cells by T cells initiates subsequent rounds of antigen presentation, T cell stimulation, trafficking and infiltration into tumours reflects not only the complexity of human immunity, but also the array of tumour immune evasion capabilities.[5 6 44] The strong therapeutic activities of CXD101-ICB combination therapy, therefore, stem from the concomitant restoration of multiple rate-limiting steps of the cancer-immunity cycle. First, CXD101 systemically hyperacetylases the regulatory regions of IRGs including *STAT1*, the crucial meditator of IFNγ pathway. This epigenomic priming works in tandem with the IFNγ signal released by CTLs,[47] which are prevented from the development of the exhausted phenotype by checkpoint blockade,[48] to synergistically activate IRGs encoding chemokines and MHC class-I complex critical for lymphocyte recruitment and tumour cell visibility, respectively. Second, CXD101 treatment also opens and primes chromatin with H3K27ac at the *GSDME* promoter and enhancer for transcriptional reactivation, leading to CTL-mediated GSDME cleavage and induction of pyroptosis, an inflammatory form of cell death that further promotes infiltration and activation of antitumour innate and adaptive immune cells.[49] As GSDME silencing by promoter hypermethylation also occurs in some human cancers,[50] pyroptosis may be epigenetically exploited in a tumour-specific manner to reinstate the cancer-immunity cycle and amplify the antitumour responses to ICB therapy.

Intriguingly, we found that IFNγ/STAT1 signalling is prerequisite for GSDME-mediated pyroptosis in vitro and in vivo. Unlike GSDMB expression which can be directly upregulated by IFNγ,[51] the cleavage of CXD101-induced GSDME is dependent on the

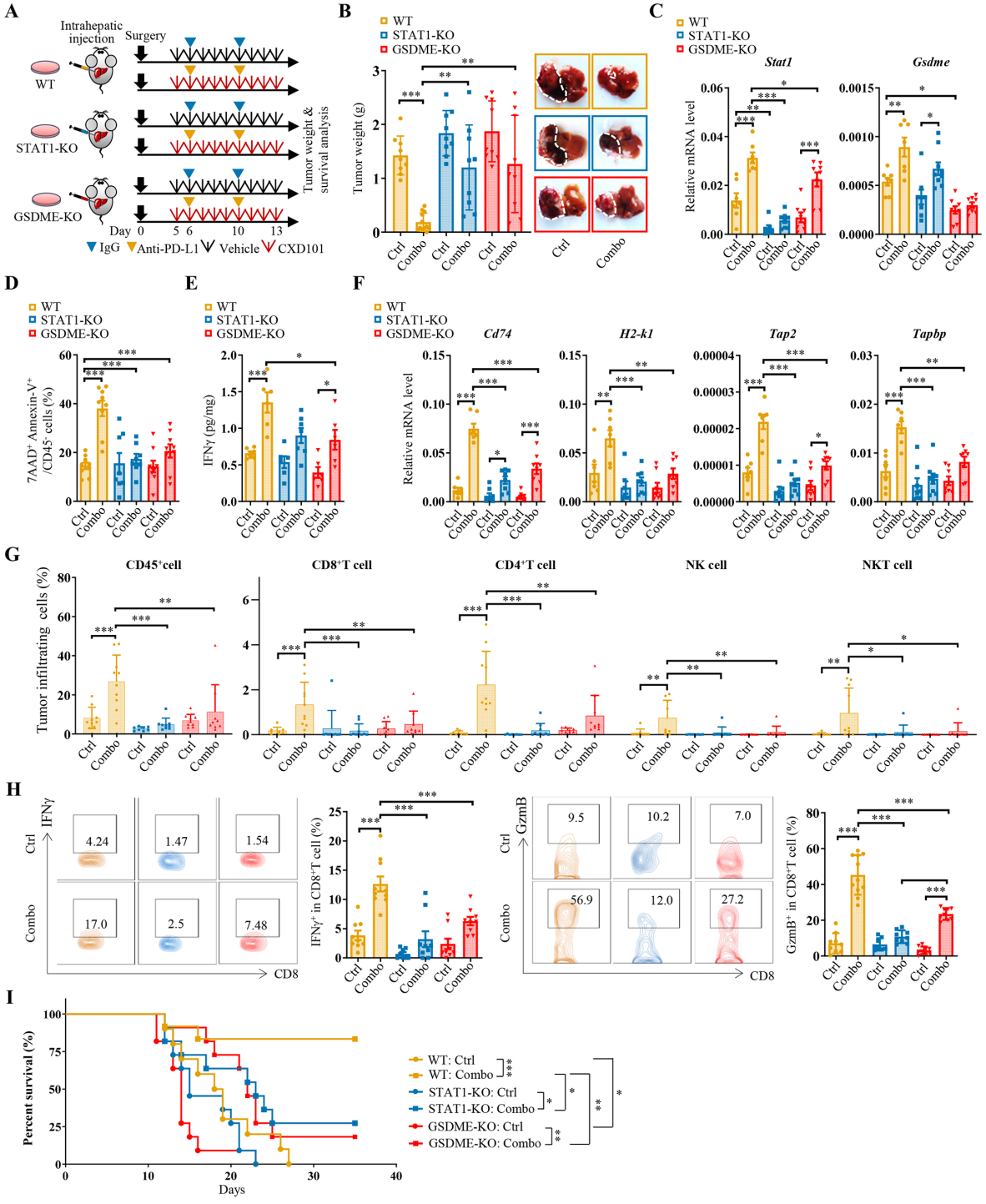

Figure 7 Deletion of tumourous STAT1 or GSDME abolishes the antitumour effects of CXD101 and anti-PD-L1 combination therapy. (A) Treatment schedule of CXD101 and anti-PD-L1 antibody in C57BL/6 mice bearing the indicated Hepa1-6-PD-L1R tumours. (B) Tumour weights and representative images of livers and tumours from indicated groups are shown (n=9–12). (C) RT-qPCR analyses of mRNA levels of *Stat1* and *Gsdme* in tumours from the indicated groups (n=7–8). (D) The proportions of $CD45^-7AAD^+Annexin\text{-}V^+$cells in tumours from the indicated groups were detected by flow cytometry assay (n=8–9). (E) IFNγ levels in tumours from the indicated groups were measured by ELISA assay (n=6–7). (F) RT-qPCR analyses of mRNA levels of the indicated genes in tumours from indicated groups (n=7–8). (G) Proportions (%) of tumour infiltrating $CD45^+$cells, $CD45^+CD3^+CD8^+$T cells, $CD45^+CD3^+CD4^+$T cells, $CD45^+NK1.1^+$NK cells and $CD45^+CD3^+NK1.1^+$NKT cells of total cells in the indicated tumours were determined by flow cytometry (n=8–10). (H) Representative flow cytometry dot plots and proportions of $IFN\gamma^+$ or $GZMB^+$ cells in tumour infiltrating $CD8^+$T cells from the indicated groups are shown (n=8–10). (I) Kaplan-Meier survival analysis of mice from the indicated groups (n=10–12). Data are represented as mean±SD. Statistical significance was assessed by one-way ANOVA with Holm-Sidak's multiple comparisons correction. *p<0.05; **p<0.01; ***p<0.001. ANOVA, analysis of variance.

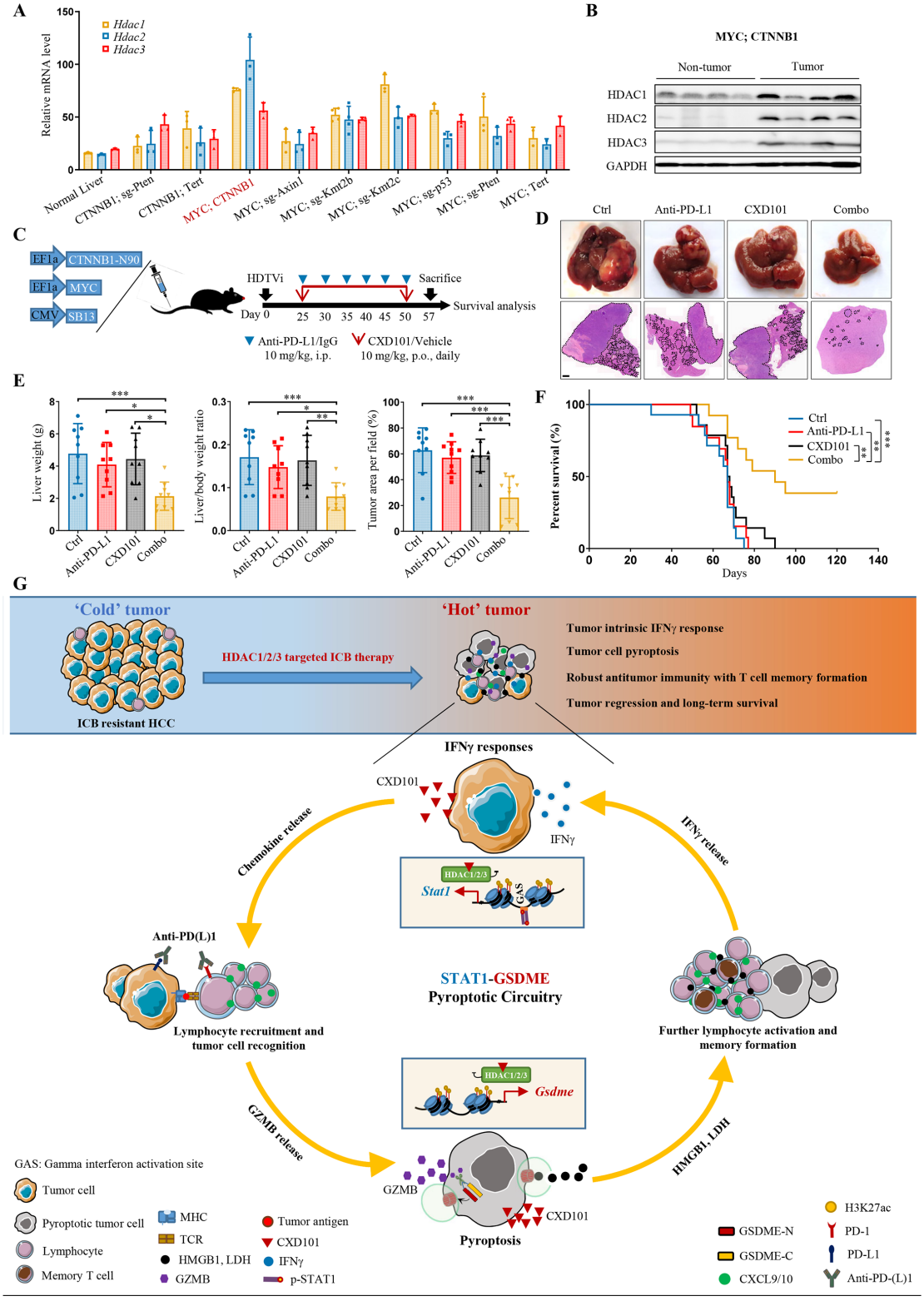

Figure 8 CXD101 synergies with anti-PD-L1 antibody to suppress tumourigenicity in spontaneous HDAC1/2/3^{high} HCC model. (A) mRNA levels of *Hdac1*, *Hdac2* and *Hdac3* in normal livers or the indicated HCC tumours were extracted from the published RNA-seq data (GSE148379). (B) Western blot analysis of HDAC1, HDAC2 and HDAC3 protein levels in MYC^{high} and CTNNB1^{mut} tumour and non-tumour liver tissues isolated from mice. GAPDH was used as loading control. (C) Treatment schedule of CXD101 and anti-PD-L1 antibody in C57BL/6 mice bearing MYC^{high} and CTNNB1^{mut} tumours by HDTVi of the indicated plasmids. (D) Representative photos (top) and H&E staining images (bottom) of livers and tumours from the indicated groups are shown. Scale bars, 1000 µm. Tumour areas are circled by black dotted lines. (E) Tumour burden in indicated groups was evaluated by liver weight, liver weight vs body weight ratio and tumour area per slide calculated from H&E images. (F) Kaplan-Meier survival analysis of mice from the indicated groups in MYC^{high} and CTNNB1^{mut} HCC model (n=13–14). (G) A summary schematic of this study. Data are represented as mean±SD. Statistical significance was assessed by one-way ANOVA with Tukey's multiple comparisons correction for (E) and by two-sided log-rank (Mantel-Cox) test for (F). *p<0.05, **p<0.01, ***p<0.001. ANOVA, analysis of variance; HCC, hepatocellular carcinoma; HDTVi, hydrodynamic tail-vein injection.

IFNγ/STAT1 axis, possibly due to the necessity of tumour cell recognition before GZMB release by cytotoxic $CD8^+$T cells.[52] The immunogenic cell death in turn fuels more lymphocyte-derived IFNγ and GZMB in the TME to reinforce the STAT1-GSDME pyroptotic circuitry. Notably, the deletion of either reciprocally regulated player in the circuit abolished the therapeutic efficacy of our combination targeting strategy, further highlighting the significance of the cooperative and synergistic remodelling of cancer-intrinsic epigenomic landscape and immune-excluded TME in the generation of an optimal antitumour immunity.

There are limitations to our study. The relatively small cohort of patients in our phase-II study (NCT03419481) may preclude the potential predictive power of HDACs for ICB responsiveness, although TIDE analysis of TCGA dataset was performed to verify the findings. While we have applied single-cell multiomics to characterise the role of chromatin accessibility in therapy-induced antitumour immunity, we cannot decode the histone modification profiles in tumour heterogeneity using the current bulk approach. Recent advancements in high-throughput single-cell ChIP-seq[53] may enable identification of a subcluster of IFNγ-responsive tumour cells with specific chromatin states and transcription factors responsible for epigenetic reprogramming through motif analysis of the enriched regions. As the majority of HCC develops in liver fibrosis, in which the peritumoural stromal and myeloid cell components form a barricade to restrict T cell immunity,[54 55] orthotopic mouse models using cell lines may not fully reflect the immune-excluded immunotype.[44] The validated therapeutic benefits of CXD101 plus ICB treatment in the HDTVi spontaneous HCC model warrant further investigation in the context of fibrosis-associated HCC.

As we have recently shown that CXD101 treatment could increase MHC class-I and MHC class-II gene expressions in dendritic cells leading to antigen presentation,[56] it is worthwhile to determine the direct effects of CXD101 on immune cells integral in the cancer-immunity cycle. While the T_{EM} cells were elevated in the tumour rechallenge model, our pilot ex vivo study did not show obvious changes in memory T cell proportions by direct CXD101 and ICB treatment (online supplemental figure 22). CXD101 treatment also did not exhibit direct effect on $CD8^+$T cell cytotoxicity in the OVA-specific OT-I cell model (online supplemental figure 23). Further studies using T cell-selective knockout approach are warranted to clarify the impact of class-I HDACs on T cell responses.

The identification of clinically druggable targets that restrict antitumour immunity is required to develop potential combination therapies. Using single-cell transcriptomic data on patients with HCC treated with anti-PD-1 therapy and newly established preclinical ICB-resistant models, we identified class-I HDACs as key epigenetic drivers restricting the amplification of the antitumour immunity cycle, thereby contributing to the immune-refractory feature of TME and ICB resistance. The successful conversion of the immune-excluded into an inflamed immunotype through epigenetic activation of STAT1-GSDME pyroptotic circuitry provides a mechanistic basis of CXD101 plus anti-PD-1 treatment in patients with ICB-resistant HCC. We envision that application of single-cell multiomics analysis in the new phase-II clinical trial (NCT05873244) will advance precision medicine with immuno-epigenetic therapy through identification of predictive biomarkers for responsiveness and durability.

Author affiliations
[1]School of Biomedical Sciences, The Chinese University of Hong Kong, Hong Kong, China
[2]Department of Liver Surgery, Renji Hospital Affiliated to Shanghai Jiao Tong University, School of Medicine, Shanghai, China
[3]Department of Clinical Pharmacy, Guangzhou Medical University, Guangzhou, China
[4]Department of Clinical Oncology, The Chinese University of Hong Kong, Hong Kong, China
[5]Department of Anatomical and Cellular Pathology, The Chinese University of Hong Kong, Hong Kong, China
[6]School of Biomedical Sciences, Li Ka Shing Faculty of Medicine, The University of Hong Kong, Hong Kong, China
[7]Nuffield Division of Clinical and Laboratory Sciences, University of Oxford, Oxford, UK
[8]Department of Oncology, The University of Oxford, Oxford, UK
[9]Lee Kong Chian School of Medicine, Nanyang Technological University, Singapore
[10]State Key Laboratory of Digestive Disease, The Chinese University of Hong Kong, Hong Kong, China

X Stephanie Ma @stephaniema912 and Man Tong @caroltong92

Acknowledgements We acknowledge Professor Lars Zender and Professor Tim F. Greten for their kind gift of the RIL-175 HCC cell line. We would also thank Professor Xin Chen for providing us with HDTVi plasmids (pT3-EF1a-c-Myc and pCMV-SB13). We also acknowledge Professor Patrick Ming-Kuen Tang for the generous gift of NK92 cell line. The scRNA-seq and single-cell multiomics were performed at the Single Cell Omics Core, School of Biomedical Sciences, Faculty of Medicine, The Chinese University of Hong Kong.

Contributors Study concept and design: YT, SLC and AS-LC; Data acquisition and analysis: YT, HW, CZ, YanL, ZX, SiyunC, JW, PP-CW, WY, ZL, JLu, ShufenC, LZ, YF, WW-YS-T, BY, YingnanL, JLiang, LL, JSLV, WR, TTK, HL, JZ, HS, SLC and AS-LC; Clinical resources: SLC and K-FT; Bioinformatics analysis: HW; Writing of manuscript: YT and AS-LC; Material support: SM, DK and NLT; Critical review of manuscript: JZ and AS-LC; Supervision: MT, QX, JJYS, SLC and AS-LC; Funding acquisition: SM, DK, NLT, JJYS, SLC and AS-C. AS-LC is the guarantor.

Funding This project is supported by the General Research Fund (14119023, 14120621 and 14115820), Theme-based Research Scheme (T11-706/18-N), Research Impact Fund (R7022-20), the Li Ka Shing Foundation (CUHK_2021), the CUHK Strategic Seed Funding for Collaborative Research Scheme (NL/SSFCRS2022/0672/22en) and the NSFC/RGC Joint Research Scheme 2023/24 (N_CUHK456/23). We also acknowledge support (funding and study medications) by IngenOx Therapeutics (CUHK_2019) and Merck Sharp and Dohme (MSD-IIS 55253) for the preclinical and clinical studies, respectively.

Competing interests The authors declare no conflicts of interest related to this work, except for the following declarations. SLC serves as an advisory member for AstraZeneca, MSD, Eisai, BMS, Ipsen and Hengrui, received research funds from MSD, Eisai, Ipsen, SIRTEX and Zailab, and honoraria from AstraZeneca, Eisai, Roche, Ipsen and MSD.

Patient and public involvement Patients and/or the public were not involved in the design, or conduct, or reporting, or dissemination plans of this research.

Patient consent for publication Not applicable.

Ethics approval This study involves human participants and animal subjects, which was approved by the Joint CUHK- NTEC Clinical Research Ethics Committee (CREC 2017.465-T) and The Chinese University of Hong Kong Animal Experimentation Ethics Committee (20-038-GRF), respectively.

Provenance and peer review Not commissioned; externally peer reviewed.

Data availability statement Data are available on reasonable request.

ORCID iDs
Jianxin Liang http://orcid.org/0000-0002-6636-0872
Stephanie Ma http://orcid.org/0000-0002-2029-7943

Jingying Zhou http://orcid.org/0000-0002-9740-6159
Joseph J Y Sung http://orcid.org/0000-0003-3125-5199
Alfred Sze-Lok Cheng http://orcid.org/0000-0001-5503-5882

REFERENCES

1 Llovet JM, Kelley RK, Villanueva A, *et al*. Hepatocellular carcinoma. *Nat Rev Dis Primers* 2021;7:6.
2 Donne R, Lujambio A. The liver cancer immune microenvironment: Therapeutic implications for hepatocellular carcinoma. *Hepatology* 2023;77:1773–96.
3 Finn RS, Qin S, Ikeda M, *et al*. Atezolizumab plus Bevacizumab in Unresectable Hepatocellular Carcinoma. *N Engl J Med* 2020;382:1894–905.
4 Sangro B, Sarobe P, Hervás-Stubbs S, *et al*. Advances in immunotherapy for hepatocellular carcinoma. *Nat Rev Gastroenterol Hepatol* 2021;18:525–43.
5 Chen DS, Mellman I. Elements of cancer immunity and the cancer-immune set point. *Nature New Biol* 2017;541:321–30.
6 Sharma P, Hu-Lieskovan S, Wargo JA, *et al*. Primary, Adaptive, and Acquired Resistance to Cancer Immunotherapy. *Cell* 2017;168:707–23.
7 Parker BS, Rautela J, Hertzog PJ. Antitumour actions of interferons: implications for cancer therapy. *Nat Rev Cancer* 2016;16:131–44.
8 Ivashkiv LB. IFNγ: signalling, epigenetics and roles in immunity, metabolism, disease and cancer immunotherapy. *Nat Rev Immunol* 2018;18:545–58.
9 Kalbasi A, Ribas A. Tumour-intrinsic resistance to immune checkpoint blockade. *Nat Rev Immunol* 2020;20:25–39.
10 Liu H, Golji J, Brodeur LK, *et al*. Tumor-derived IFN triggers chronic pathway agonism and sensitivity to ADAR loss. *Nat Med* 2019;25:95–102.
11 Haber PK, Castet F, Torres-Martin M, *et al*. Molecular Markers of Response to Anti-PD1 Therapy in Advanced Hepatocellular Carcinoma. *Gastroenterology* 2023;164:72–88.
12 Terekhanova NV, Karpova A, Liang W-W, *et al*. Epigenetic regulation during cancer transitions across 11 tumour types. *Nat New Biol* 2023;623:432–41.
13 Mohammad HP, Barbash O, Creasy CL. Targeting epigenetic modifications in cancer therapy: erasing the roadmap to cancer. *N Med* 2019;25:403–18.
14 West AC, Johnstone RW. New and emerging HDAC inhibitors for cancer treatment. *J Clin Invest* 2014;124:30–9.
15 Kelly-Sell MJ, Kim YH, Straus S, *et al*. The histone deacetylase inhibitor, romidepsin, suppresses cellular immune functions of cutaneous T-cell lymphoma patients. *Am J Hematol* 2012;87:354–60.
16 Truong AS, Zhou M, Krishnan B, *et al*. Entinostat induces antitumor immune responses through immune editing of tumor neoantigens. *J Clin Invest* 2021;131:e138560.
17 Oh SJ, Lee H-J, Song K-H, *et al*. Targeting the NANOG/HDAC1 axis reverses resistance to PD-1 blockade by reinvigorating the antitumor immunity cycle. *J Clin Invest* 2022;132:e147908.
18 Que Y, Zhang X-L, Liu Z-X, *et al*. Frequent amplification of HDAC genes and efficacy of HDAC inhibitor chidamide and PD-1 blockade combination in soft tissue sarcoma. *J Immunother Cancer* 2021;9:e001696.
19 Yang W, Feng Y, Zhou J, *et al*. A selective HDAC8 inhibitor potentiates antitumor immunity and efficacy of immune checkpoint blockade in hepatocellular carcinoma. *Sci Transl Med* 2021;13:eaaz6804.
20 Lim B, Lin Y, Navin N. Advancing Cancer Research and Medicine with Single-Cell Genomics. *Cancer Cell* 2020;37:456–70.
21 Xiong Z, Chan SL, Zhou J, *et al*. Targeting PPAR-gamma counteracts tumour adaptation to immune-checkpoint blockade in hepatocellular carcinoma. *Gut* 2023;72:1758–73.
22 Sun R, Zhang Z, Bao R, *et al*. Loss of SIRT5 promotes bile acid-induced immunosuppressive microenvironment and hepatocarcinogenesis. *J Hepatol* 2022;77:453–66.
23 Li Y, Zhang X, Zhu S, *et al*. HDAC10 Regulates Cancer Stem-Like Cell Properties in KRAS-Driven Lung Adenocarcinoma. *Cancer Res* 2020;80:3265–78.
24 Li G, Choi JE, Kryczek I, *et al*. Intersection of immune and oncometabolic pathways drives cancer hyperprogression during immunotherapy. *Cancer Cell* 2023;41:304–22.
25 Jiang P, Gu S, Pan D, *et al*. Signatures of T cell dysfunction and exclusion predict cancer immunotherapy response. *Nat Med* 2018;24:1550–8.
26 Eyre TA, Collins GP, Gupta A, *et al*. A phase 1 study to assess the safety, tolerability, and pharmacokinetics of CXD101 in patients with advanced cancer. *Cancer* 2019;125:99–108.
27 Booth SW, Eyre TA, Whittaker J, *et al*. A Phase 2a cohort expansion study to assess the safety, tolerability, and preliminary efficacy of CXD101 in patients with advanced solid-organ cancer expressing HR23B or lymphoma. *BMC Cancer* 2021;21:851.
28 Karin N, Razon H. Chemokines beyond chemo-attraction: CXCL10 and its significant role in cancer and autoimmunity. *Cytokine* 2018;109:24–8.
29 Ma S, Zhang B, LaFave LM, *et al*. Chromatin Potential Identified by Shared Single-Cell Profiling of RNA and Chromatin. *Cell* 2020;183:1103–16.
30 Han H, Cho J-W, Lee S, *et al*. TRRUST v2: an expanded reference database of human and mouse transcriptional regulatory interactions. *Nucleic Acids Res* 2018;46:D380–6.
31 Creyghton MP, Cheng AW, Welstead GG, *et al*. Histone H3K27ac separates active from poised enhancers and predicts developmental state. *Proc Natl Acad Sci U S A* 2010;107:21931–6.
32 Basha G, Omilusik K, Chavez-Steenbock A, *et al*. A CD74-dependent MHC class I endolysosomal cross-presentation pathway. *Nat Immunol* 2012;13:237–45.
33 Platanias LC. Mechanisms of type-I- and type-II-interferon-mediated signalling. *Nat Rev Immunol* 2005;5:375–86.
34 Chen X, He W-T, Hu L, *et al*. Pyroptosis is driven by non-selective gasdermin-D pore and its morphology is different from MLKL channel-mediated necroptosis. *Cell Res* 2016;26:1007–20.
35 Broz P, Pelegrín P, Shao F. The gasdermins, a protein family executing cell death and inflammation. *Nat Rev Immunol* 2020;20:143–57.
36 Lu C, Guo C, Chen H, *et al*. A novel chimeric PD1-NKG2D-41BB receptor enhances antitumor activity of NK92 cells against human lung cancer H1299 cells by triggering pyroptosis. *Mol Immunol* 2020;122:200–6.
37 Yang HG, Kang MC, Kim TY, *et al*. Discovery of a novel natural killer cell line with distinct immunostimulatory and proliferative potential as an alternative platform for cancer immunotherapy. *J Immunother Cancer* 2019;7:138.
38 Volchuk A, Ye A, Chi L, *et al*. Indirect regulation of HMGB1 release by gasdermin D. *Nat Commun* 2020;11:4561.
39 Yu P, Zhang X, Liu N, *et al*. Pyroptosis: mechanisms and diseases. *Signal Transduct Target Ther* 2021;6:128.
40 Dagogo-Jack I, Shaw AT. Tumour heterogeneity and resistance to cancer therapies. *Nat Rev Clin Oncol* 2018;15:81–94.
41 Molina-Sánchez P, Ruiz de Galarreta M, Yao MA, *et al*. Cooperation Between Distinct Cancer Driver Genes Underlies Intertumor Heterogeneity in Hepatocellular Carcinoma. *Gastroenterology* 2020;159:2203–20.
42 Sia D, Jiao Y, Martinez-Quetglas I, *et al*. Identification of an Immune-specific Class of Hepatocellular Carcinoma, Based on Molecular Features. *Gastroenterology* 2017;153:812–26.
43 Ruiz de Galarreta M, Bresnahan E, Molina-Sánchez P, *et al*. β-Catenin Activation Promotes Immune Escape and Resistance to Anti-PD-1 Therapy in Hepatocellular Carcinoma. *Cancer Discov* 2019;9:1124–41.
44 Mellman I, Chen DS, Powles T, *et al*. The cancer-immunity cycle: Indication, genotype, and immunotype. *Immunity* 2023;56:2188–205.
45 Benci JL, Johnson LR, Choa R, *et al*. Opposing Functions of Interferon Coordinate Adaptive and Innate Immune Responses to Cancer Immune Checkpoint Blockade. *Cell* 2019;178:933–48.
46 Litchfield K, Reading JL, Puttick C, *et al*. Meta-analysis of tumor- and T cell-intrinsic mechanisms of sensitization to checkpoint inhibition. *Cell* 2021;184:596–614.
47 Qiao Y, Giannopoulou EG, Chan CH, *et al*. Synergistic activation of inflammatory cytokine genes by interferon-γ-induced chromatin remodeling and toll-like receptor signaling. *Immunity* 2013;39:454–69.
48 Sharma P, Goswami S, Raychaudhuri D, *et al*. Immune checkpoint therapy-current perspectives and future directions. *Cell* 2023;186:1652–69.
49 Rosenbaum SR, Wilski NA, Aplin AE. Fueling the Fire: Inflammatory Forms of Cell Death and Implications for Cancer Immunotherapy. *Cancer Discov* 2021;11:266–81.
50 Zhang Z, Zhang Y, Lieberman J. Lighting a Fire: Can We Harness Pyroptosis to Ignite Antitumor Immunity? *Cancer Immunol Res* 2021;9:2–7.
51 Zhou Z, He H, Wang K, *et al*. Granzyme A from cytotoxic lymphocytes cleaves GSDMB to trigger pyroptosis in target cells. *Science* 2020;368:eaaz7548.
52 Zhang Z, Zhang Y, Xia S, *et al*. Gasdermin E suppresses tumour growth by activating anti-tumour immunity. *Nature New Biol* 2020;579:415–20.
53 Grosselin K, Durand A, Marsolier J, *et al*. High-throughput single-cell ChIP-seq identifies heterogeneity of chromatin states in breast cancer. *Nat Genet* 2019;51:1060–6.
54 Liu M, Zhou J, Liu X, *et al*. Targeting monocyte-intrinsic enhancer reprogramming improves immunotherapy efficacy in hepatocellular carcinoma. *Gut* 2020;69:365–79.
55 Liu X, Zhou J, Wu H, *et al*. Fibrotic immune microenvironment remodeling mediates superior anti-tumor efficacy of a nano-PD-L1 trap in hepatocellular carcinoma. *Mol Ther* 2023;31:119–33.
56 Liu G, Barczak W, Lee LN, *et al*. The HDAC inhibitor zabadinostat is a systemic regulator of adaptive immunity. *Commun Biol* 2023;6:102.